ELSEVIER

Thermochimica Acta 373 (2001) 59–67

thermochimica acta

www.elsevier.com/locate/tca

Thermal behavior of the amorphous precursors of the HfO_2–Fe_2O_3 system

G. Štefanić*, S. Musić

Division of Materials Chemistry, Ruđer Bošković Institute, P.O. Box 180, 10002 Zagreb, Croatia

Received 24 November 2000; accepted 16 January 2001

Abstract

The amorphous precursors of the HfO_2–Fe_2O_3 system at the HfO_2-rich side of the concentration range were prepared by the co-precipitation of the corresponding salts from aqueous solutions. The thermal behavior of the samples was followed using differential thermal analysis and X-ray diffraction at high-temperature. The differences in the phase developments during the heating of the samples in the presence of air at atmospheric pressure ($\sim 10^5$ Pa) and low pressure ($\sim 4 \times 10^{-3}$ Pa) were attributed to the influence of the oxygen vacancies introduced during calcination at low pressure. The results of phase analysis showed that Fe^{3+} ions have both a stabilizing and destabilizing influence on the high-temperature polymorphs of HfO_2. The incorporation of 10–30 mol% of Fe_2O_3 stabilized cubic hafnia during calcination in the presence of air at atmospheric pressure, but further increase of the iron content caused the destabilization of this phase. The destabilizing influence of the Fe^{3+} ions increased during calcination at low pressure. The oxygen vacancies introduced during the calcination at low pressure partially stabilized the cubic HfO_2, but this stabilizing influence significantly decreased in the samples with high iron content. The obtained results indicated that both the stabilizing and destabilizing influences of Fe^{3+} ions are related to the oxygen vacancies introduced in the HfO_2 lattice. The stabilization of the high-temperature polymorphs of HfO_2 depended on the amount of oxygen vacancies and their distribution inside the lattice. The solid solubility limits of Fe_2O_3 in HfO_2 decreased during heating at atmospheric pressure from >30 mol% at 700°C to ~2 mol% at 1000°C. The solubility of Fe_2O_3 in HfO_2 during the heating at low pressure was higher.

Keywords: HfO_2–Fe_2O_3 system; Oxygen vacancies; Solid solubility; XRD

1. Introduction

Zirconia and hafnia have very similar chemical and structural properties which are significantly different from other metal oxides. The predominantly covalent nature of Zr–O and Hf–O bonds favors the seven-fold coordination (7 CN) of Zr and Hf cations in their thermodynamically stable monoclinic polymorphs.

The high-temperature cubic and tetragonal polymorphs of ZrO_2 and HfO_2, with eight-fold coordination of cations, could be stabilized at room temperature by the incorporation of aliovalent cations [1–8]. In the case of undersized dopants, such as Fe^{3+} ions, this stabilization is not very efficient [8–15]. Aliovalent cations introduce oxygen vacancies that decrease the CN of Zr and Hf ions. Ho [16] estimated the lowest amount of oxygen vacancies required for the stabilization of cubic ZrO_2 at 6.5%. However, this estimation assumes that all the vacancies are associated with the Zr cations. Li et al. [8] investigated

* Corresponding author. Tel.: +385-01-456-1111; fax: +385-1-46-80-084.
E-mail address: stefanic@rudjer.irb.hr (G. Štefanić).

0040-6031/01/$ – see front matter
PII: S0040-6031(01)00455-5

zirconia solid solutions with trivalent dopants. They found that vacancies introduced by oversized dopants (Gd^{3+} and Y^{3+}) were located as the nearest neighbors to the Zr ions, leaving eight-fold oxygen coordination to dopant cations. On the other hand, undersized dopants (Fe^{3+} and Ga^{3+}) compete with the Zr ions for oxygen vacancies, resulting in the six-fold oxygen coordination of dopant cations and the less effective stabilization of the cubic and tetragonal phases [8]. Štefanić et al. [15,17] investigated the influence of oxygen on the thermal behavior of the ZrO_2 [17] and the system ZrO_2–Fe_2O_3 [15]. It was found that calcination at very low pressure introduces oxygen vacancies into the ZrO_2 lattice, resulting in the stabilization of *c*-ZrO_2. The incorporation of Fe^{3+} ions caused the transition of this cubic phase into the phase structurally closely related to *m*-ZrO_2. These results indicated that aliovalent undersized dopants have both a stabilizing and destabilizing influence on the high-temperature polymorphs of zirconia [15]. Contrary to the system ZrO_2–Fe_2O_3, the system HfO_2–Fe_2O_3 was much less investigated. In the present work, we used in situ phase analysis to investigate phase development during the heating of the amorphous precursors to the HfO_2–Fe_2O_3 system in the presence and absence of oxygen. The obtained results were compared with the previously obtained results for the ZrO_2–Fe_2O_3 system [15].

2. Experimental

Aqueous solutions with the appropriate molar fraction of $HfOCl_2{\cdot}8H_2O$ and $FeCl_3{\cdot}6H_2O$ salts were coprecipitated by adding 25% NH_3 aqueous up to pH ∼10.4. The solid phase was separated from the mother liquid using an ultra-speed centrifuge (operational speed of up to 20,000 rpm), then washed repeatedly with doubly distilled water and dried at 90°C for 24 h. The notation of the samples and their initial molar compositions are given in Table 1.

In order to examine the influence of air on phase development, the prepared samples were separated into two parts. The first part of the samples was heated under the atmospheric pressure of air (∼10^5 Pa) and the second part under low air pressure (∼4×10^{-3} Pa).

Phase developments during the heating of both parts of the samples were examined in situ using X-ray powder diffraction (Philips counter diffractometer, model MPD 1880) with monochromatized Cu Kα radiation. The prepared samples were deposited onto the platinum heating strip inside the high-temperature chamber (Paar HTK 10) attached to the diffractometer. The samples were heated to, a chosen temperature at the rate of 5°C min^{-1} and stabilized for 20 min before the measurement. The temperature was measured by Pt/10% RhPt thermocouple. XRD patterns were scanned over the 2θ range from 23 to 37°, which contains the most prominent diffraction lines of *m*-, *t*-, *c*-HfO_2, α-Fe_2O_3 and Fe_3O_4. The data were collected in steps of 0.02° (2θ) with, a fixed counting time of 5 s.

The thermal behavior of the first part of the samples was also followed using differential thermal analysis. Differential thermal analysis was performed up to 950°C with a scanning rate of 10°C min^{-1}, using the standard instrumentation.

Table 1
The notation of the samples and the initial molar compositions

Sample	$x(HfO_2)$	$x(Fe_2O_3)$
HF0	1	–
HF1	0.99	0.01
HF2	0.97	0.03
HF3	0.90	0.10
HF4	0.80	0.20
HF5	0.70	0.30
HF6	0.50	0.50

3. Results

The results of phase analysis obtained during the heating of the samples in the presence of air at atmospheric pressure (∼10^5 Pa) and low pressure (∼4×10^{-3} Pa) are given in Table 2. Characteristic parts of the XRD patterns of some samples obtained during these heating procedures are shown in Figs. 1–5.

3.1. Heating at atmospheric pressure

Prior to the temperature treatments, all the samples were amorphous. Phase developments during the thermal treatment of the samples HF0, HF1 and HF2 were shown to be very similar. Heating of these samples caused their crystallization into the H_m phase,

Table 2
The results of in situ phase analysis during the heating of the samples in the presence of air at atmospheric pressure ($\sim 10^5$ Pa) and low pressure ($\sim 4 \times 10^{-3}$ Pa)[a]

Sample	Temperature (°C)	Phase composition	
		Atmospheric pressure	Low pressure
HF0	RT	Amorphous	Amorphous
	500	H_m	Amorphous
	600	H_m	Amorphous
	700	H_m	Amorphous + H_m + H_c
	800	H_m	H_m + H_c + amorphous
	900	H_m	–
	1000	H_m	H_m + H_c
	1200		H_m
HF1	RT	Amorphous	–
	500	H_m	Amorphous
	600	H_m	Amorphous
	700	H_m	Amorphous + H_m + H_c
	800	H_m	H_m + H_c + amorphous
	900	H_m	H_m + H_c
	1000	H_m	H_m + H_c
	1200	–	H_m
HF2	RT	Amorphous	–
	500	H_m + amorphous	Amorphous
	600	H_m	Amorphous
	700	H_m	Amorphous + H_c
	800	H_m	Amorphous + H_c
	900	H_m	–
	1000	H_m + F_H	H_c + H_m
	1200	–	H_m
HF3	500	Amorphous	Amorphous
	600	H_c	Amorphous
	700	H_c	Amorphous
	800	H_c + H_m	Amorphous + H_c
	900	H_m + F_H	Amorphous + H_c + H_m
	1000	H_m + F_H	H_c + H_m
	1200	–	H_m + H_c
HF4	600	Amorphous	–
	700	H_c	Amorphous
	800	H_c + H_m	Amorphous + H_c
	900	H_m + F_H + H_c	Amorphous + H_c + H_m
	1000	H_m + F_H	H_c + H_m
	1200	–	H_c + H_m + F
HF5	500	Amorphous	–
	600	–	Amorphous
	700	H_c	Amorphous + H_c + H_m
	800	–	H_c + H_m + amorphous
	900	H_m + F_H	H_m + H_c + F_H
	1000	H_m + F_H	H_m + F_H + F_M + H_c
	1200	–	H_m + F_H + M
HF6	300	Amorphous + F_H	–
	500	Amorphous + F_H + H_m	Amorphous + F_H + H_m
	700	H_c + F_H + H_m	H_m + H_c + F_M + F_H
	800	H_m + F_H + H_c	H_m + F_M + H_c + F
	900	H_m + F_H	H_m + F_M + F_H + H_c
	1000	H_m + F_H	H_m + F_M + F_H
	1200	–	H_m + F_M + F

[a] Description: H_m = phase structurally similar to m-HfO_2, H_c = phase structurally similar to c-HfO_2, F_H = phase structurally similar to α-Fe_2O_3, F_M = phase structurally similar to Fe_3O_4.

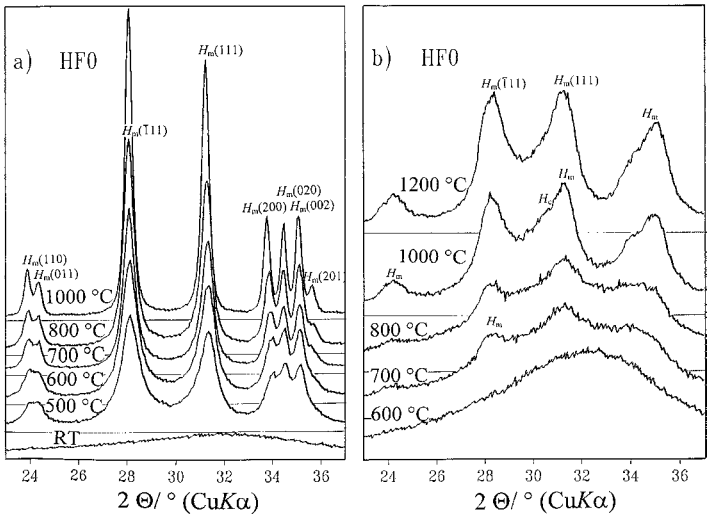

Fig. 1. Characteristic part of XRD patterns of the HF0 sample obtained during the heating in the presence of air at: (a) pressure of $\sim 10^5$ Pa; (b) pressure of $\sim 4 \times 10^{-3}$ Pa.

closely structurally related to *m*-HfO_2. In all three samples, the first sign of the crystal phase appeared at 500°C. However, the sample HF2 was still predominantly amorphous, which indicates a somewhat higher crystallization temperature. Further heating of the samples up to 1000°C caused an increase and sharpening of the diffraction lines of the H_m phase (Figs. 1–3). The XRD pattern of the sample HF2 obtained at 1000°C also contained small diffraction lines of the F_H phase, closely structurally related to α-Fe_2O_3 (Fig. 3). The presence of this phase indicated that the solubility of the Fe_2O_3 in the HfO_2 lattice decreased below 3 mol%.

The first sign of the diffraction lines indicating the stabilization of the high-temperature polymorphs of HfO_2 appeared in the XRD pattern of the sample HF3

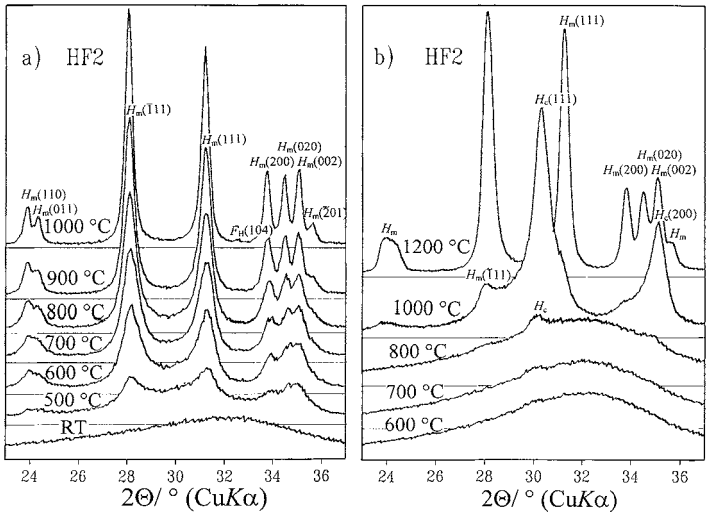

Fig. 2. Characteristic part of XRD patterns of the HF2 sample obtained during the heating in the presence of air at: (a) pressure of $\sim 10^5$ Pa; (b) pressure of $\sim 4 \times 10^{-3}$ Pa.

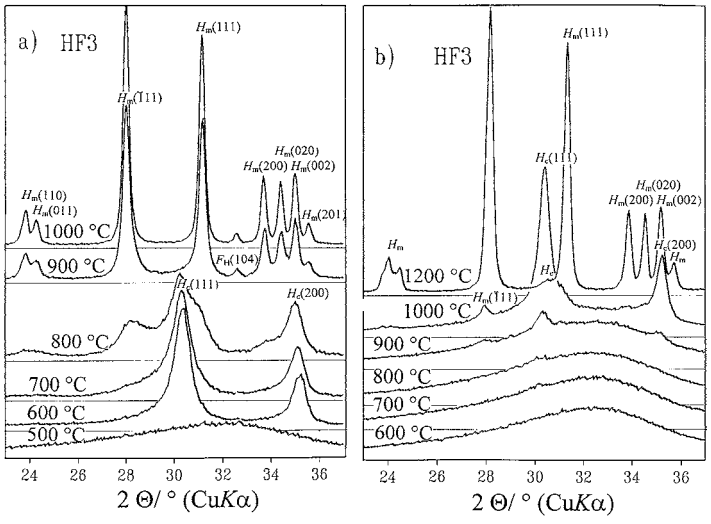

Fig. 3. Characteristic part of XRD patterns of the HF3 sample obtained during the heating in the presence of air at: (a) pressure of $\sim 10^5$ Pa; (b) pressure of $\sim 4 \times 10^{-3}$ Pa.

(10 mol% of Fe_2O_3) recorded at 600°C. The H_c phase, closely structurally related to c-HfO_2, was the only phase present at 600 and 700°C. The temperature increase caused the appearance of the H_m phase and its increase on the account of the H_c phase. At 900°C, the H_c phase disappeared and the F_H phase appeared. Similar phase development occurred during the heating of the samples HF4 and HF5 (20 and 30 mol% of Fe_2O_3), but in these samples crystallization into the H_c phase occurred at 700°C and the F_H phase appeared at 800°C. As in the XRD pattern of the sample HF3, the diffraction lines of the H_c phase disappeared in the XRD pattern of the sample HF5 recorded at 900°C (Fig. 4). However, the diffraction lines of this phase were still present in the corresponding XRD pattern of the sample HF4. Small diffraction lines of the F_H and

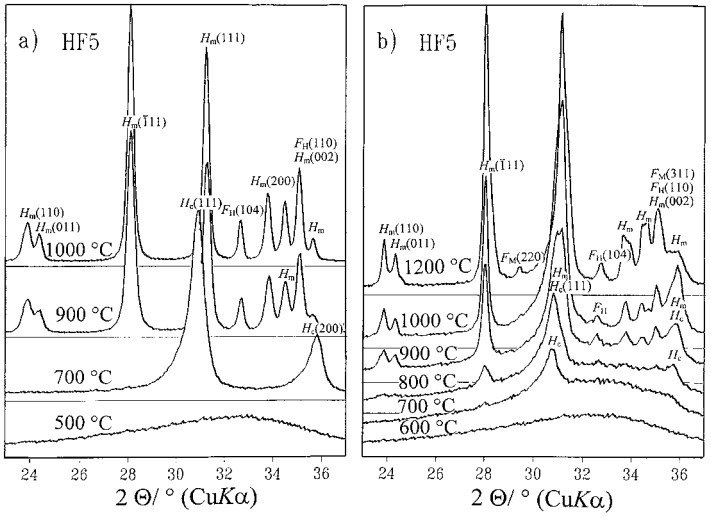

Fig. 4. Characteristic part of XRD patterns of the HF5 sample obtained during the heating in the presence of air at: (a) pressure of $\sim 10^5$ Pa; (b) pressure of $\sim 4 \times 10^{-3}$ Pa.

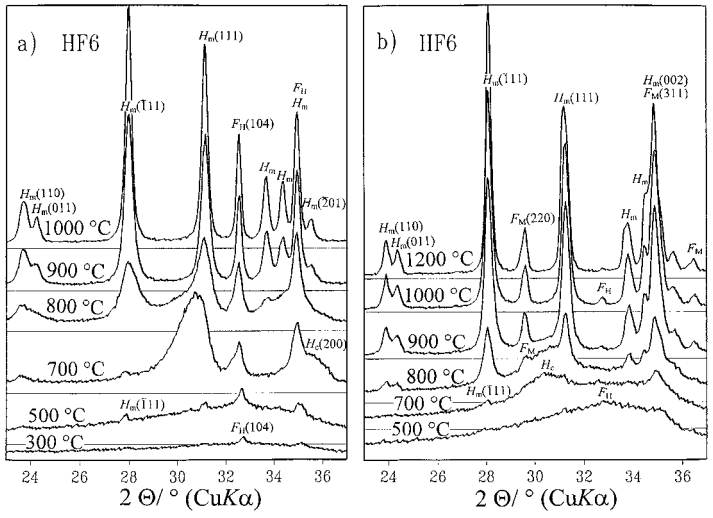

Fig. 5. Characteristic part of XRD patterns of the HF6 sample obtained during the heating in the presence of air at: (a) pressure of $\sim 10^5$ Pa; (b) pressure of $\sim 4 \times 10^{-3}$ Pa.

H_m phases appeared in the XRD patterns of the sample HF6 (50 mol% of Fe_2O_3) recorded at 300 and 500°C (Fig. 5). However, the sample was still predominantly amorphous. The amorphous fraction of the sample crystallized at 700°C into the H_c phase. Further temperature increase caused the $H_c \rightarrow H_m$ transition (completed at 900°C) followed by an increase of the F_H phase.

The DTA curves of all the samples contained one broad endothermic peak with the maximum at ~150°C, resulting from dehydration; and one sharp exothermic peak, resulting from the crystallization of the amorphous materials. The temperature of the crystallization increased with an increase of iron content from 515°C for pure HfO_2 to 720°C for a sample with 50 mol% of Fe_2O_3 (Table 3). The samples with 10–30 mol% of Fe_2O_3 contained an additional exothermic peak between 920 and 895°C resulting from the phase transition that caused the appearance of the F_H phase.

3.2. Heating at low pressure

The phase developments of the samples HF0, HF1 and HF2 during this thermal treatment were similar but significantly different from the corresponding phase development caused by heating at atmospheric pressure. The first sign of the crystal phase in these samples appeared at 700°C but the samples were still predominantly amorphous. The crystallization process occurred very slowly and the amorphous phase was still present at 800°C. The XRD patterns of the crystallization products contained very broad diffraction lines of both the H_m and H_c phases. The increase in temperature caused the $H_c \rightarrow H_m$ transition and the H_c phase finally disappeared at 1200°C. The first sign of the crystal phase in the XRD patterns of the samples HF3 and HF4 appeared at 800°C, indicating a further increase of the crystallization temperature. The content of the H_c phase in the crystallization products of these samples increased but the H_m phase was still present. The $H_c \rightarrow H_m$ transition caused by the

Table 3
The results of DTA obtained during the heating of the samples in the presence of air at atmospheric pressure

Sample	Exothermic peak	
	Crystallization (°C)	Phase transition (°C)
HF0	515	–
HF1	545	–
HF2	575	–
HF3	640	920
HF4	690	895
HF5	705	895
HF6	720	–

increase of the heating temperature occurred much more slowly than that observed during heating at atmospheric pressure. The XRD pattern of the sample HF4 recorded at 1200°C contained diffraction lines of the H_c and H_m phases (H_c was still the dominant phase) and also small diffraction lines of the F_H phase. The phase development of the samples HF5 and HF6 indicated that further increase of the iron content caused a decrease of the crystallization temperature and the stability of the H_c phase. The first crystallization product of the sample HF5, containing both the H_c and H_m phases, appeared at a temperature ~100°C lower (700°C) than the sample HF4. The increase of the heating temperature caused the decrease and disappearance of the H_c phase and the appearance of two additional crystal phases, the F_H phase at 900°C and the F_M phase, closely structurally related to Fe_3O_4, at 1000°C.

At 500°C, the sample HF6 was predominantly amorphous but the presence of small diffraction lines of the F_H and H_m phases in the corresponding XRD pattern indicated a further decrease of the crystallization temperature. Crystallization of the amorphous fraction of the sample at 700°C caused the appearance of two additional crystal phases, phases H_c and M. The content of the H_c phase was smaller than that of the H_m phase. Further increase of the temperature caused the decrease and disappearance of the H_c phase (900°C) and the increase of the F_M phase.

3.3. Solubility of Fe_2O_3

Regardless of the heating procedure, the solubility of Fe_2O_3 in the HfO_2 lattice decreased with the increase of the heating temperature. During heating at atmospheric pressure, the solid solubility limits of Fe_2O_3 in HfO_2 were estimated from the dependence of the diffraction line intensities of the F_H phase on the initial content of Fe_2O_3, and by extrapolation to the zero intensity. The terminal solid solubility limits of Fe_2O_3 in HfO_2 were >30 mol% at 700°C, ~8 mol% after calcination at 900°C and ~2 mol% after calcination at 1000°C. The solubility of Fe_2O_3 in the HfO_2 lattice increased during heating at low pressure. However, the precise determination of the terminal solid solubility limits was difficult to obtain due to the presence of two iron phases, phases F_H and F_M.

4. Discussion

In our previous investigation [15] it was shown that the amorphous precursors of the system ZrO_2–Fe_2O_3 with >30 mol% of Fe_2O_3 are single co-gels. These co-gels crystallized during heating at atmospheric pressure into a ZrO_2-type solid solution with extended capability for the incorporation of Fe^{3+} ions [15]. A similar result was obtained in the present work for the HfO_2–Fe_2O_3 system. The increase of the crystallization temperature with the increase of the iron content and the very high solubility of the iron in the first crystallization product (>30 mol% of Fe_2O_3) indicated that the amorphous samples with >30 mol% of Fe_2O_3 are single co-gels. These co-gels crystallized into the metastable phases with extended capability for the formation of solid solutions.

Phase development during the heating of the samples strongly depends on the air pressure. Heating at low air pressure makes the crystallization of the amorphous samples more difficult and therefore the crystallization temperatures of the samples with Fe_2O_3 content of up to 10 mol% increased by >200°C (Table 2). Further increase of the iron content caused a decrease in these temperature differences, which completely disappeared in the sample with 50 mol% of Fe_2O_3. Besides the influence on the crystallization temperature, heating at low air pressure influenced the phase composition of the samples. This influence also depended on the amount of iron present in the samples. Our previous investigation showed that the presence of Fe^{3+} ions has both a stabilizing and destabilizing influence on the high-temperature polymorphs of ZrO_2 [15]. Which of these two opposite influences prevails depends on the iron content and the heating procedure used.

The stabilization of high-temperature polymorphs of HfO_2 was more difficult to obtain than that of ZrO_2, and therefore the phase development of the system HfO_2–Fe_2O_3 differs from the corresponding phase development of the system ZrO_2–Fe_2O_3. Regardless to that, the results from both systems lead to the same conclusion about the influence of Fe^{3+} ions.

Unlike the ZrO_2-type solid solutions [15], the incorporation of up to 3 mol% of Fe_2O_3 could not stabilize high-temperature polymorphs of HfO_2 during heating in the presence of air at atmospheric pressure. However, heating of the same samples at low pressure

caused the appearance of the H_c phase, which in the case of the sample with 3 mol% of Fe_2O_3 becomes the dominant one. These results clearly showed that heating at low air pressure caused the partial stabilization of the high-temperature polymorphs of HfO_2. However, the same heating procedure has the opposite effect on the samples with a higher amount of iron.

The incorporation of 10–30 mol% of Fe_2O_3 introduced high enough oxygen vacancies for the complete stabilization of the H_c phase during heating at atmospheric pressure (Table 2). On the other hand, heating of the same samples at low air pressure caused only the partial stabilization of this phase. The presence of the H_m phase showed that additional oxygen vacancies, introduced by heating at low air pressure, caused phase segregation. This segregation can be attributed to the nonuniform distribution of the oxygen vacancies. The exchange of oxygen between the lattice and the atmosphere occurred through the surface of the grains [18–20] and therefore the concentration of the oxygen vacancies introduced by heating at low pressure was higher near the surface. Nonuniform distribution of the vacancies caused nonuniform distribution of the Fe^{3+} ions, which tend to associate with these vacancies, causing phase segregation and partial destabilization of the H_c phase. This phase segregation probably also caused the decrease of the crystallization temperature in the samples with 30 and 50 mol% of Fe_2O_3 (Table 2).

The destabilizing influence of Fe^{3+} ions on the high-temperature polymorphs of HfO_2 was even more clearly shown in the sample HF6 (50 mol% of Fe_2O_3). Regardless of the heating procedure, the first crystallization products of this sample contained the H_m phase. In the case of the product obtained during heating in a vacuum, the H_m phase was the dominant one. These results, in agreement with previous results from the ZrO_2–Fe_2O_3 system [15], show that above a certain limit the further increase of the iron content caused the destabilization of the high-temperature polymorphs of HfO_2 and ZrO_2. In the case of heating at atmospheric pressure, this limit corresponded to the solid solubility limit of Fe_2O_3 in the HfO_2 or ZrO_2 lattice; while in the case of heating at low pressure (the absence of oxygen and moisture), this limit decreased due to phase segregation. The iron content above the solubility limits had no influence on the amount of the oxygen vacancies introduced and therefore could only destabilize the high-temperature polymorphs of HfO_2 and ZrO_2.

5. Conclusion

The results of this study showed that amorphous samples with >30 mol% of Fe_2O_3 are single co-gels that crystallize into an HfO_2-type solid solution with extended capability for the incorporation of Fe^{3+} ions. The solid solubility limits of Fe_2O_3 in HfO_2 decreased during heating in the presence of air at atmospheric pressure, from >30 mol% at 700°C to ~2 mol% at 1000°C. Phase developments during the heating of the samples strongly depended on the air pressure. Heating at low pressure introduced oxygen vacancies that caused the increase of the crystallization temperature and the partial stabilization of cubic HfO_2. However, these influences decreased in the samples with high iron content. The results showed that Fe^{3+} ions have both a stabilizing and destabilizing influence on the high-temperature polymorphs of HfO_2. These influences were shown to be connected to the oxygen vacancies introduced in the HfO_2 lattice. The stabilization of the high-temperature polymorphs of HfO_2 depended on the amount of oxygen vacancies and their distribution inside the lattice.

References

[1] P. Duran, C. Pascual, J. Mater. Sci. 19 (1984) 1178.
[2] D.-J. Kim, S.-H. Hyun, S.-G. Kim, M. Yashima, J. Am. Ceram. Soc. 77 (2) (1994) 597.
[3] M. Yashima, H. Takahashi, K. Ohtake, T. Hirose, M. Kakihana, H. Arashi, Y. Ikuma, Y. Suzuki, M. Yoshimura, J. Phys. Chem. Solids 157 (1996) 289.
[4] M. Yashima, N. Ishizawa, M. Yoshimura, J. Am. Ceram. Soc. 75 (1992) 1541.
[5] M.F. Trubelja, V.S. Stubican, Solid State Ionics 49 (1991) 89.
[6] V.V. Kharton, A.A. Yaremchenko, E.N. Naumovich, F.M.B. Marques, J. Solid State Electrochem. 4 (2000) 243.
[7] C.J. Howard, R.J. Hill, B.E. Reichert, Acta Crystallogr. Sect. B 44 (1988) 116.
[8] P. Li, I.-W. Chen, J.E. Penner-Hahn, J. Am. Ceram. Soc. 77 (1994) 118.
[9] S. Davison, R. Kershaw, K. Dwight, A. Wold, J. Solid State Chem. 73 (1988) 47.
[10] F.J. Berry, M.H. Loretto, M.R. Smith, J. Solid State Chem. 83 (1989) 91.

[11] I.B. Inwang, F. Chyad, I.J. McColm, J. Mater. Chem. 5 (1995) 1209.
[12] S. Popović, B. Gržeta, G. Štefanić, I. Czakó-Nagy, S. Musić, J. Alloys Comp. 241 (1996) 10.
[13] G. Štefanić, S. Musić, S. Popović, K. Nomura, J. Mol. Struct. 480/481 (1999) 627.
[14] S. Popović, G. Štefanić, S. Musić, Mater. Lett. 31 (1997) 19.
[15] G. Štefanić, B. Grežta, S. Musić, Mater. Chem. Phys. 65 (2000) 216.
[16] S.M. Ho, Mater. Sci. Eng. 54 (1982) 23.
[17] G. Štefanić, B. Gržeta, S. Popović, S. Musić, Croat. Chem. Acta. 72 (1999) 395.
[18] R. Srinivasan, T.R. Watkins, C.R. Hubbard, B.H. Davis, Chem. Mater. 7 (1995) 725.
[19] G. Štefanić, S. Musić, S. Popović, A. Sekulić, J. Mol. Struct. 408/409 (1997) 391.
[20] G. Štefanić, S. Popović, S. Musić, Mater. Lett. 36 (1998) 240.